Semi-supervised Learning of Nonrigid Deformations for Image Registration

John A. Onofrey[1(✉)], Lawrence H. Staib[1,2,3], and Xenophon Papademetris[1,3]

[1] Department of Biomedical Engineering, Yale University, New Haven, CT 06520, USA
[2] Department of Electrical Engineering, Yale University, New Haven, CT 06520, USA
[3] Department of Diagnostic Radiology, Yale University, New Haven, CT 06520, USA
{john.onofrey,lawrence.staib,xenophon.papademetris}@yale.edu

Abstract. The existence of large medical image databases have made large amounts of neuroimaging data accessible and freely available to the research community. In this paper, we harness both the vast quantity of unlabeled anatomical MR brain scans from the 1000 Functional Connectomes Project (FCP1000) database and the smaller, but richly-annotated brain images from the LONI Probabilistic Brain Atlas (LPBA40) database to learn a statistical deformation model (SDM) of the nonrigid transformations in a semi-supervised learning (SSL) framework. We make use of 39 LPBA40 labeled MR datasets to create a set of supervised registrations and augment these results with a set of unsupervised registrations using 1247 unlabeled MRIs from the FCP1000. We show through leave-one-out cross validation that SSL of a nonrigid SDM results in a registration algorithm with significantly improved accuracy compared to standard, intensity-based registration, and does so with a 99 % reduction in transformation dimensionality.

Keywords: Image registration · Nonrigid · Semi-supervised learning · Statistical deformation model · Principal component analysis

1 Introduction

Nonrigid spatial normalization of different subjects to a common reference space has utility in a variety of medical imaging applications, for instance in population studies of functional brain imaging [5] and in atlas-based brain segmentation [1]. However, nonrigid image registration of different subjects is a challenging task made difficult, in part, by highly variable anatomical structure. Accurate anatomical alignment requires nonrigid transformations with a large number of degrees of freedom (DoFs). Inter-subject image registration with such high-dimensionality is an ill-posed optimization problem.

Statistical deformations models (SDMs) have the potential to reduce the dimensionality of the nonrigid transformations by learning the subspace or manifold in which these transformations exist. SDMs attempt to analyze anatomical

B. Menze et al. (Eds.): MCV 2013, LNCS 8331, pp. 13–23, 2014.
DOI: 10.1007/978-3-319-05530-5_2,

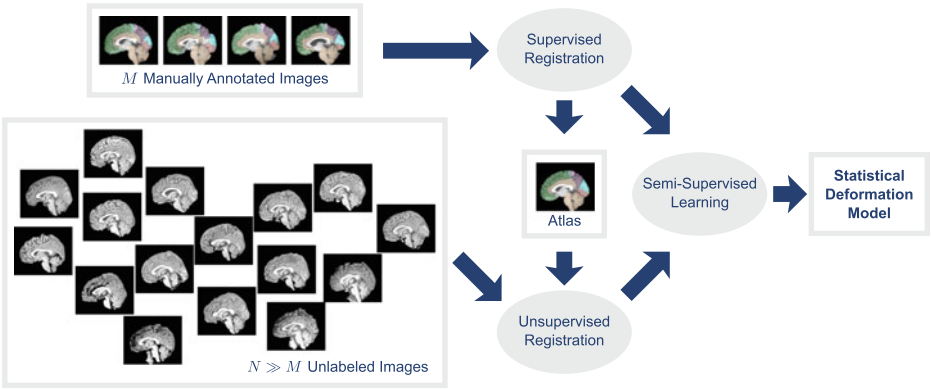

Fig. 1. Our semi-supervised learning approach makes use of both a small number of gold-standard, manually-annotated image samples and a large number of unlabeled image samples. We use the labeled VOIs in the M annotated images to perform a type of supervised nonrigid registration, from which we create a reference atlas composed of average anatomy and majority-vote label images. We then nonrigidly register the N unlabeled images to the atlas in an unsupervised manner using standard, intensity-only registration. Finally, we perform a principal component analysis of the supervised and unsupervised transformations to learn a statistical deformation model.

variation by modeling the nonrigid image deformations from a set of training images. Rueckert *et al.* [10] proposed principal component analysis (PCA) of nonrigid deformations to create a low-dimensional, linear orthonormal basis of high-dimensional registrations. Other authors have made use of PCA-based SDMs in this manner for low-dimensional image registration [7] and as a registration regularization prior [15]. However, if the SDM is not trained using accurate registrations, the utility of the model is questionable. Onofrey *et al.* [8] demonstrate improved PCA SDM performance by training with a set of richly-annotated images. Regardless of training the SDM with labeled or unlabeled data, previous PCA-based SDMs offer relatively underwhelming registration performance due to PCA's inability to model the high-dimensional transformation's variance with orders of magnitude fewer number of training samples.

Thankfully, large medical image databases containing vast amounts of neuroimaging data, such as the 1000 Functional Connectomes Project International Neuroimaging Data-Sharing Initiative [2] (FCP1000), offer an accessible and freely available source of SDM training samples. In contrast, smaller databases like the UCLA Laboratory of Neuroimaging (LONI) Probabilistic Brain Atlas (LPBA40) [12] contain relatively few images, but incorporate richly-annotated information, such as gold-standard manually-segmented volumes of interest (VOIs). Datasets containing such rich information are labor intensive and expensive to create. In this paper, we leverage both the vast quantity of unlabeled anatomical MR brain scans from the FCP1000 dataset and the small, but labeled brain images from the LPBA40 dataset to learn a SDM of nonrigid

registration in a semi-supervised learning (SSL) framework. The concepts of using both labeled and unlabeled training data for SSL are widely applicable for classification problems [3], but its use for image registration is novel, to the best of our knowledge. As illustrated in Fig. 1, we make use of 39 of the LPBA40's labeled MR datasets to create a set of supervised registrations. We augment this supervised sample set with a second set of unsupervised registrations using 1247 unlabeled MRIs from the FCP1000. To the best of our knowledge, no prior work has made use 1286 MRIs to learn a SDM for image registration. We show through leave-one-out cross validation that semi-supervised learning (SSL) our nonrigid statistical deformation model (SDM) results in a nonrigid registration algorithm with significantly improved accuracy compared to standard, intensity-based registration, and does so with a 99 % reduction in transformation dimensionality.

2 Methods

Our proposed SSL nonrigid registration framework requires both supervised and unsupervised training registration samples. For both types of registrations, we use a free-form deformation (FFD) transformation model [11]. The FFD B-spline control point displacements parameterize a dense nonrigid deformation field $T(\mathbf{x}) \in \mathbb{R}^3$ at all voxels $\mathbf{x} \in \Omega \subset \mathbb{R}^3$, where Ω is the reference image volume in three dimensions. We rewrite this transformation as a column vector of P concatenated FFD control point displacements, $\mathbf{d} \in \mathbb{R}^{3P}$.

We denote the set of nonrigid transformations computed using a *supervised* registration procedure $D_s = \{\mathbf{d}_m | m = 1, \ldots, M\}$ and the set of nonrigid transformations estimated using an *unsupervised* registration approach $D_u = \{\mathbf{d}_{M+n} | n = 1, \ldots, N\}$. Sections 2.1 and 2.2 describe our supervised and unsupervised registration methodologies, respectively. We registered all $M+N$ sample images to a common reference space (described in Sect. 2.1) with $181 \times 217 \times 181$ volume with $1\,\text{mm}^3$ resolution. For an FFD with 5 mm control point spacing, this volume required $P = 60,236$ control points, thus each deformation had 180,708 DoFs in 3D. Together, the sets D_s and D_u comprise our SDM's SSL training set. Section 2.3 describes our SDM and how we subsequently used that SDM to nonrigidly register images not included in the training set.

2.1 Supervised Nonrigid Registration

To create our set of supervised nonrigid registrations D_s, we make use of a database containing gold-standard, manually-segmented VOIs to constrain our deformations with respect to these VOIs [8]. The LPBA40 database [12] contains 40 anatomical, skull-stripped brain MR images I_i, $i = 1, \ldots, 40$, with 56 annotated VOIs. In order to calculate our nonrigid registrations using a common reference domain, we first register all 40 images to the MNI Colin 27 brain. We then select subject 1 to be used as an initial reference template image I_1 for nonrigid registration of the remaining subjects. Using an integrated intensity and point-feature nonrigid registration algorithm [9], we nonrigidly register

the remaining $M = 39$ subjects to our reference. This algorithm uses a FFD transformation model with 5 mm control point spacing and minimizes the sum of squared differences (SSD) similarity measure while penalizing misalignment of the VOI surface points according to the robust point matching algorithm [4]. The labeled image data allows for accurate normalization of anatomical image intensities, which motivates using SSD for these registrations. We denote these transformations $T_{i \rightsquigarrow 1}, i = 2, \ldots, 40$ ($i \rightsquigarrow j$ denotes nonrigid registration from space i to j). Our choice of reference image biases the registrations to that subject's particular anatomy. To correct for this, we compute the mean transformation $\bar{T} = \frac{1}{M} \sum_{i=2}^{40} T_{i \rightsquigarrow 1}$ and apply the inverse transformation $\bar{T}^{-1}$ to subject 1 to create a deformation bias-corrected (DBC) image $I_{\text{DBC}} = \bar{T}^{-1} \circ I_1$, where $\circ$ is the transformation operator. We then re-register the M subjects to I_{DBC} using the same integrated nonrigid registration as before, and denote these transformations $T_{i \rightsquigarrow \text{DBC}}$. As this set of transformations leverages annotated VOIs and we constrain our registration procedure to align these VOIs, the FFD control point displacements of these transformations constitute our set of supervised registrations $D_s = \{\mathbf{d}_m | m = 1, \ldots, M\}$.

In addition to creating D_s, we also create an atlas composed of an anatomical image $I_{\text{Atlas}} = \frac{1}{M-1} \sum_{i=2}^{40} T_{i \rightsquigarrow \text{DBC}} \circ I_i$ and a corresponding VOI label image found using a majority-vote of the 39 transformed subject VOIs. I_{Atlas} is a representative template image for the set of nonrigid FFD transformations with 5 mm control point spacing. We thus use I_{Atlas} as the reference image for our unsupervised registrations described in the following section.

2.2 Unsupervised Nonrigid Registration

We require a large number of unsupervised samples to supplement our small set of supervised registrations. From the FCP1000 database [2], we culled $N = 1247$ unlabeled, anatomical brain MR images of healthy, normal subjects. First, we register all images to our common reference space, I_{Atlas}, using an affine transformation $T_{n \rightarrow \text{Atlas}}, n = 1, \ldots, N$ ($i \rightarrow j$ denotes rigid registration from space i to j) by maximizing the normalized mutual information (NMI) similarity metric [13]. Following affine registration, we then estimate the nonrigid deformation of all N brains to I_{Atlas}.

Using the same FFD nonrigid transformation model with 5 mm control point spacing as in Sect. 2.1, we nonrigidly register each subject by maximizing NMI. However, unlike the skull-stripped LPBA40 images in Sect. 2.1, these images have no manual correction, and thus artifacts, e.g. the optic nerve, remain in some images (as can be seen in Fig. 1). Such artifacts present challenges for intensity-based registration methods. Rather than manually correcting these poor segmentations, we perform weighted nonrigid registration [14] that preferentially weights the brain region during the calculation of NMI. For this, we create a brain weight mask image by first dilating I_{Atlas}'s brain mask and then smoothing with a Gaussian kernel. The resulting transformations $T_{n \rightsquigarrow \text{Atlas}}$ and their respective FFD control point displacements comprise our set of unsupervised registrations $D_u = \{\mathbf{d}_{M+n} | n = 1, \ldots, N\}$.

2.3 Semi-supervised Statistical Deformation Model Registration

Using both the supervised and unsupervised registration sets, D_s and D_u, respectively, we create a statistical deformation model (SDM) of nonrigid FFD transformation [10]. A principal component analysis of the deformations $\mathbf{d}_i, i = 1, \ldots, M+N$ gives a linear approximation of the deformation distribution

$$\mathbf{d} = \bar{\mathbf{d}} + \mathbf{\Phi}\mathbf{w} \tag{1}$$

where $\bar{\mathbf{d}} = \frac{1}{M+N}\sum_{i=1}^{M+N}\mathbf{d}_i$ is the mean deformation of the $M+N$ training registrations, $\mathbf{\Phi} = (\phi_1|\ldots|\phi_K) \in \mathbb{R}^{3P\times K}$ is the matrix of orthogonal eigenvectors, and $\mathbf{w} \in \mathbb{R}^K$ is a vector of model coefficients. The number of training samples determines the number of eigenvectors such that $K = \min\{M+N, 3P\}$. The k-th eigenvalue λ_k estimates the sample variance along the eigenvector ϕ_k, and we sort them in decreasing order $\lambda_1 \geq \lambda_2 \geq \ldots \geq \lambda_K$. A SDM using K_v parameters accounts for $0 \leq v \leq 100\,\%$ of the model's cumulative variance

$$\sum_{k=1}^{K_v}\lambda_k \leq v\sum_{k=1}^{K}\lambda_k.$$

Thus, using the first K_v coefficients of $\mathbf{w}$ in Eq. 1 provides a low-dimensional parameterization (K_v DoFs) of a high-dimensional FFD $\mathbf{d}$, which we denote $T_{\mathrm{SDM}_v}(\mathbf{x};\mathbf{w})$ for all points $\mathbf{x}$ in the reference image domain Ω.

To nonrigidly register a new image I to our reference image I_{Atlas}, we use the SDM from Eq. 1 to optimize the cost function

$$\hat{T}_{\mathrm{SDM}_v} = \arg\max_{\mathbf{w}} J(I_{\mathrm{Atlas}}, T_{\mathrm{SDM}_v}(\cdot;\mathbf{w}) \circ I). \tag{2}$$

Here, J is the NMI similarity metric evaluated throughout the image volume. We solve Eq. 2 using conjugate gradient optimization with a hierarchical multi-resolution image pyramid.

3 Results and Discussion

We tested our SSL SDM by performing a series of *leave-one-out* tests. For each supervised registration $\mathbf{d}_i \in D_s$, we recomputed the SDM in Sect. 2.3 by leaving the i-th deformation out of Eq. 1. We did not recompute I_{Atlas} as in Sect. 2.1 for each leave-one-out test because the single subject's exclusion had negligible effect on the mean intensity image. Section 3.1 presents results showing the SDM's ability to reconstruct each of the $i = 1, \ldots, 39$ deformations. Section 3.2 then shows how well the SDM registered $\mathbf{d}_i$'s corresponding anatomical image I_i in the LPBA40 dataset to I_{Atlas} using Eq. 2. For comparison, we created another SDM using standard, unsupervised-only registration training samples. We trained this unsupervised SDM with $N+M$ training samples by replacing the LPBA40 supervised registrations in D_s with unsupervised registrations of the same images using our methodology from Sect. 2.2. We also compared our

results to standard, intensity-only FFD registration using 5 mm control point spacing, which we denote FFD_5.

To evaluate registration accuracy in both sections, we calculated the mean Dice overlap (MDO) of the $V = 56$ VOIs with respect to the atlas labels

$$\text{MDO}_i = \frac{1}{V} \sum_{v \in V} \frac{2|(I_i)_v \cap (I_{\text{Atlas}})_v|}{|(I_i)_v| + |(I_{\text{Atlas}})_v|}$$

where $(A)_v$ denotes the v-th VOI from image A. We found MDO to be a suitable summary statistic to quantify registration performance rather than analyze each individual VOI Dice overlap separately. Furthermore, since our supervised registration framework constrained VOI boundaries to align and a certain amount of registration uncertainty remains at locations away from those boundaries, our use of Dice overlap more appropriately measures accurate alignment of VOI boundaries than a residual sum of square transformation error.

We implemented our code on the GPU using the CUDA parallel programming platform as part of BioImage Suite [6]. The eigensystem in Eq. 1 may be precomputed ahead of the registration, and can then be loaded into the algorithm to avoid unnecessarily repetitious PCA computation. We compared the computation time of our approach to standard FFD_5.

3.1 SSL SDM Reconstructions

For each leave-one-out test, we tested the SDM's ability to reconstruct the i-th subject's deformation $\mathbf{d}_i$ by rewriting Eq. 1 and solving

$$\hat{\mathbf{d}}_i = \bar{\mathbf{d}}_i + \mathbf{\Phi}_i \mathbf{\Phi}_i^T (\mathbf{d}_i - \bar{\mathbf{d}}_i)$$

where $\hat{\mathbf{d}}_i$ is a least-squares approximation to $\mathbf{d}_i$, and we calculated $\bar{\mathbf{d}}_i$ and $\mathbf{\Phi}_i$ using $\mathbf{d}_j, \forall j \neq i$. We resliced image I_i using $\hat{\mathbf{d}}_i$ and computed the MDO_i. Figure 2 compares the reconstruction performance of the SSL SDM and the unsupervised SDM using different numbers of unsupervised registration training samples, $0 \leq N \leq 1247$. We selected the N samples sequentially, without randomization. Figure 2 also shows how the SSL SDMs performed using only supervised samples, i.e. $N = 0$.

As to be expected, reconstruction performance increased with the number of samples. However, the inclusion of only a small number of supervised registration samples, $M = 38$ in the case of leave-one-out testing, significantly increased the reconstructive capabilities of the SDM. This observed increase in SDM reconstruction performance is the result of the supervised training samples increasing the PCA model space's variance. Using standard FFD_5 registration as a reference for comparison (MDO $=78.09 \pm 1.26$, shown in Table 1), the SSL SDM had approximately the same level of registration performance using $N = 400$ unsupervised samples, and significantly better performance using the full $N = 1247$ unsupervised samples. On the other hand, the unsupervised SDM required $N = 1285$ samples to achieve the equivalent performance as FFD_5.

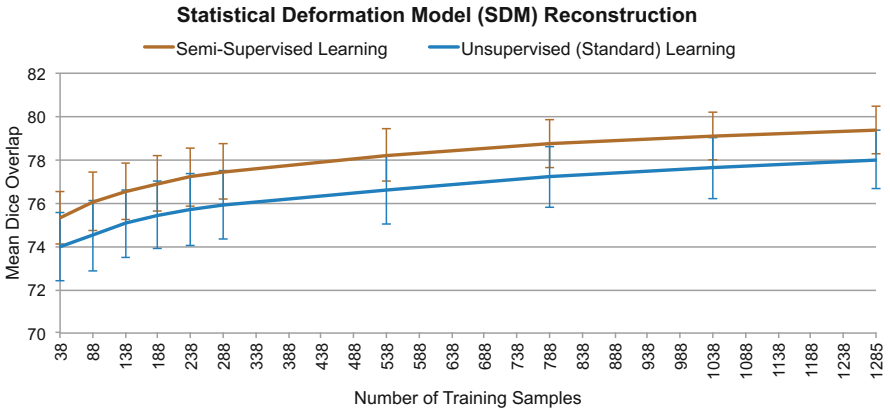

Fig. 2. Mean dice overlap values for leave-one-out transformation reconstructions as a function of the number of training samples. The inclusion of a few, 39, supervised registration samples significantly increased the SDM's reconstruction abilities. These results represent an upper bound for SDM registration performance. The plotted values are the mean with error bars of one standard deviation.

We also noted that the MDO curves in Fig. 2 appeared to be continuing to increase with inclusion of additional training samples. These reconstructions provided a theoretical upper bound for SDM registration performance, and Sect. 3.2 presents how well our proposed SDM effectively registered images in practice.

3.2 SSL SDM Registration

Having shown theoretical improvements, we now demonstrate that our approach also works in practice. For each of the 39 leave-one-out test cases, we compared registration using 4 methods: (i) SSL SDM with $M = 38, N = 1247$ training samples, (ii) unsupervised SDM with $M = 0, N = 1285$ training samples, (iii) supervised SDM with $M = 38, N = 0$ training samples, and (iv) standard, intensity FFD_5. For each of the SDM's, we registered I_i using the first K_v eigenvectors that contained the first $v = 25, 50, 75, 90, 95, 99, 100\,\%$ percentage of variance (for the supervised SDM, we replaced $v = 25$ with $33\,\%$ to avoid using 0 eigenvectors) and computed MDO_i. For each percentage of variance v, SSL SDM required $K_v = 5, 19, 76, 228, 390, 800, 1285$ eigenvectors, respectively, as shown on the left of Fig. 3. Similarly, the unsupervised SDM required $K_v = 4, 19, 77, 236, 405, 817, 1285$ eigenvectors and the supervised SDM required $K_v = 1, 2, 11, 23, 29, 35, 38$ eigenvectors. The number of eigenvectors defined the dimensionality of the nonrigid deformation. Figure 3 plots the cumulative variance v of the SSL SDM as function of the number of eigenvectors used, K_v.

Figure 3 also shows MDO as function of v for each of the three SDM types. As seen in Sect. 3.1, SSL SDM significantly outperformed unsupervised SDM for all values of v ($p \leq 8.9 \times 10^{-8}$, two-tailed paired t-test). The supervised SDM performed worse than both SSL and unsupervised SDMs, with the exception

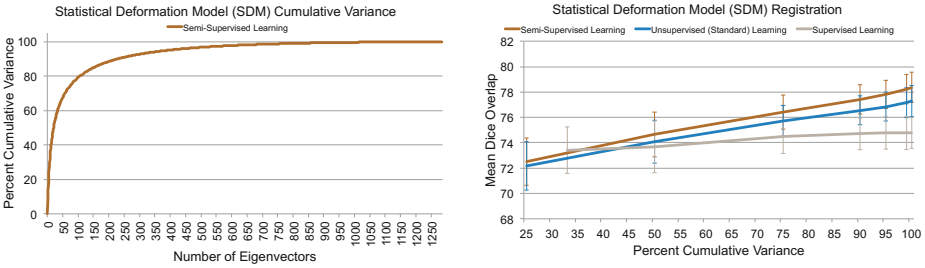

Fig. 3. The left plot shows SSL SDM's cumulative variance as function of the number of eigenvectors. On the right, we show SDM registration performance using mean dice overlap as a function of SDM cumulative variance. We plot results for SDMs trained using: (i) SSL with $M = 38, N = 1247$ samples, (ii) unsupervised learning with $N = 1285$ samples, and (iii) supervised learning with $M = 38$ samples.

Table 1. Leave-one-out registration results comparing our proposed SSL SDM registration method using 100 % of the variance, i.e. all PCA eigenvectors, with SDMs using supervised and unsupervised training samples alone, as well as standard, intensity FFD registration using 5 mm control point spacing. Reported values are mean±std MDO and minimum MDO for 39 subjects. Computational times were measured using an NVIDIA GeForce GTX 580 GPU.

Method	DoFs	MDO	Min MDO	Compute Time (m)
SSL SDM	1285	$\mathbf{78.35 \pm 1.19}$	**75.90**	36.62 ± 7.60
Unsupervised SDM	1285	77.28 ± 1.22	73.85	33.10 ± 5.74
Supervised SDM	38	74.77 ± 1.23	70.83	0.55 ± 0.07
Intensity FFD_5	180,708	78.09 ± 1.26	74.08	73.85 ± 1.39

of using $v = 0.33$, i.e. a single eigenvector. These results were to be expected given the small number of training samples, $M = 38$, and the large percentage of cumulative variance modeled by the first eigenvector. However, we observed that the SSL SDM was unable to fully achieve the theoretical reconstructive performance of the SDM. While our registration algorithm's performance closely followed that of the SSL reconstructions, our use of NMI as a similarity metric appeared to yield a non-convex cost function with local minima that prevented our algorithm from attaining the SDM's theoretical performance bound at a global minimum.

Table 1 highlights the results of our tests using $v = 100\,\%$ for each of the registration methods. In terms of MDO, our SSL SDM performed significantly better than FFD_5, unsupervised SDM, and supervised SDM using two-tailed, paired t-tests ($p \leq 0.02$). Most impressively, the SDM achieved more accurate registration than FFD_5 while reducing the dimensionality of the nonrigid deformation from 180,708 to 1285, a 99 % reduction in DoFs. This translated to a 50 % speedup in mean computation time. Also of note is SSL SDM's worst case performance, with minimum MDO 75.90, being higher than FFD_5's minimum

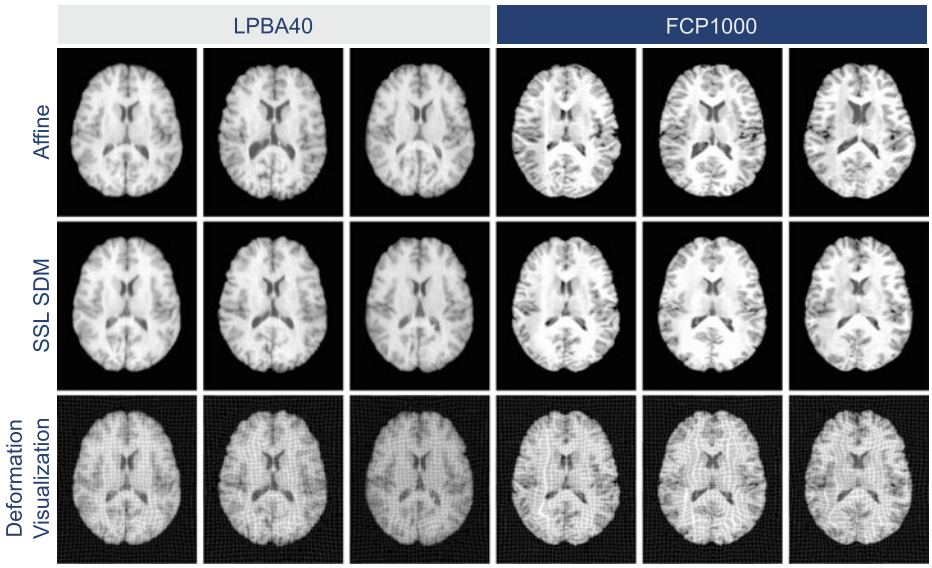

Fig. 4. Exemplar subjects and their respective registrations using our semi-supervised learning (SSL) SDM during leave-one-out tests. We show example images drawn from both the supervised (LPBA40) and unsupervised (FCP1000) training datasets. The first row shows the original images after affine registration to our atlas reference (not pictured). The second row shows the same images after SSL SDM registration using 1285 eigenvectors. The third row overlays a 5 mm isotropic grid to visualize the nonrigid deformation.

MDO 74.08. By constraining the registration transformation to be from the learned space of deformations, the SDM prevented the registration from becoming stuck in worse local minima. Figure 4 illustrates the SSL SDM registration results for some exemplar images drawn from both the supervised (LPBA40) and unsupervised (FCP1000) training data.

4 Conclusion

We demonstrate the utility of using an existing large-scale medical image database to augment the learning of nonrigid SDMs. By training a SDM in a semi-supervised manner using both a small set of accurate, supervised registrations and a large set of registrations of unknown quality, we show significantly improved registration performance with a 99 % reduction in registration DoFs. The constraints afforded by the learned SDM not only serve to better register images but also to avoid poor registration that could otherwise occur with unconstrained and unsupervised registration algorithms. While our registration algorithm in Eq. 2 does not bias the deformations towards the mean deformation, it may be of interest to implement the algorithm in a Bayesian framework and compare

registration performance and robustness. We plan to further validate our algorithm using other databases that contain annotated brain images and to test the SDM's generalizability.

Our future work aims to explore methods for nonlinear dimensionality reduction, and compare these results to that of linear PCA. However, the results presented in this paper show that, while simple, PCA is indeed effective at modeling the high-dimensional space of nonrigid brain deformations, and that the limiting factor for a PCA-based SDM is the number of training samples used. Both our theoretical and actual SSL SDM registration results suggest that the space of nonrigid deformations between subjects is of surprisingly low dimensionality.

References

1. Aljabar, P., Heckemann, R., Hammers, A., Hajnal, J., Rueckert, D.: Multi-atlas based segmentation of brain images: atlas selection and its effect on accuracy. NeuroImage **46**(3), 726–738 (2009)
2. Biswal, B.B., et al.: Toward discovery science of human brain function. Proc. Nat. Acad. Sci. **107**(10), 4734–4739 (2010)
3. Chapelle, O., Schölkopf, B., Zien, A.: Semi-supervised Learning. MIT Press, Cambridge (2006)
4. Chui, H., Rangarajan, A.: A new point matching algorithm for non-rigid registration. Comput. Vis. Image Underst. **89**(2–3), 114–141 (2003)
5. Gholipour, A., Kehtarnavaz, N., Briggs, R., Devous, M., Gopinath, K.: Brain functional localization: a survey of image registration techniques. IEEE Trans. Med. Imaging **26**(4), 427–451 (2007)
6. Joshi, A., Scheinost, D., Okuda, H., Belhachemi, D., Murphy, I., Staib, L., Papademetris, X.: Unified framework for development, deployment and robust testing of neuroimaging algorithms. Neuroinformatics **9**, 69–84 (2011)
7. Kim, M.J., Kim, M.H., Shen, D.: Learning-based deformation estimation for fast non-rigid registration. In: IEEE Computer Society Conference on Computer Vision and Pattern Recognition Workshops, 2008, CVPRW '08, pp. 1–6 (June 2008)
8. Onofrey, J., Staib, L., Papademetris, X.: Fast nonrigid registration using statistical deformation models learned from richly annotated data. In: 2013 IEEE International Symposium on Biomedical Imaging: From Nano to Macro, pp. 576–579 (April 2013)
9. Papademetris, X., Jackowski, A.P., Schultz, R.T., Staib, L.H., Duncan, J.S.: Integrated intensity and point-feature nonrigid registration. In: Barillot, C., Haynor, D.R., Hellier, P. (eds.) MICCAI 2004. LNCS, vol. 3216, pp. 763–770. Springer, Heidelberg (2004)
10. Rueckert, D., Frangi, A., Schnabel, J.: Automatic construction of 3-D statistical deformation models of the brain using nonrigid registration. IEEE Trans. Med. Imaging **22**(8), 1014–1025 (2003)
11. Rueckert, D., Sonoda, L., Hayes, C., Hill, D., Leach, M., Hawkes, D.: Nonrigid registration using free-form deformations: application to breast MR images. IEEE Trans. Med. Imaging **18**(8), 712–721 (1999)
12. Shattuck, D., et al.: Construction of a 3D probabilistic atlas of human cortical structures. NeuroImage **39**(3), 1064–1080 (2008)
13. Studholme, C., Hill, D., Hawkes, D.: An overlap invariant entropy measure of 3D medical image alignment. Pattern Recogn. **32**(1), 71–86 (1999)

14. Suh, J., Scheinost, D., Qian, X., Sinusas, A.J., Breuer, C., Papademetris, X.: Serial nonrigid vascular registration using weighted normalized mutual information. In: 2010 IEEE International Symposium on Biomedical Imaging: From Nano to Macro, pp. 25–28 (2010)
15. Xue, Z., Shen, D., Davatzikos, C.: Statistical representation of high-dimensional deformation fields with application to statistically constrained 3D warping. Med. Image Anal. **10**(5), 740–751 (2006)

http://www.springer.com/978-3-319-05529-9

Medical Computer Vision. Large Data in Medical Imaging
Third International MICCAI Workshop, MCV 2013, Nagoya, Japan, September 26, 2013, Revised Selected Papers
Menze, B.; Langs, G.; Montillo, A.; Kelm, M.; Müller, H.; Tu, Z. (Eds.)

2014, XI, 229 p. 93 illus., Softcover
ISBN: 978-3-319-05529-9